

# EyePreserve: Identity-Preserving Iris Synthesis

Siamul Karim Khan, Patrick Tinsley, Mahsa Mitcheff, Patrick Flynn, Kevin W. Bowyer, Adam Czajka  
University of Notre Dame

{skhan22, ptinsley, mmitcheff, flynn, kwb, aczajka}@nd.edu

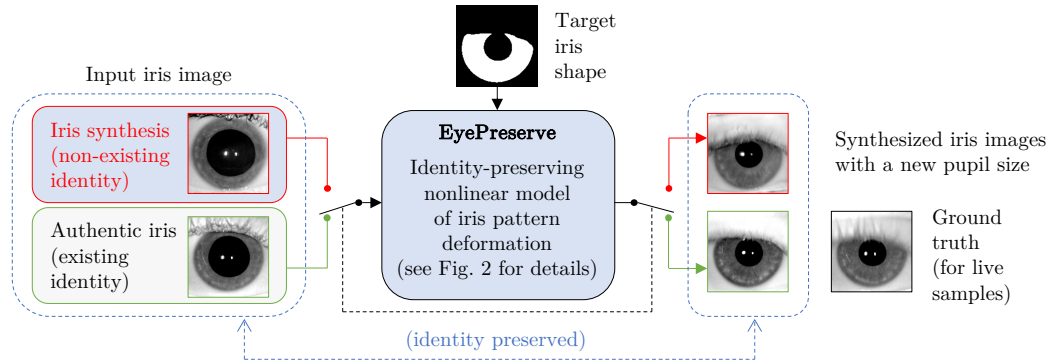


Figure 1. EyePreserve accepts an iris image (either synthetically-generated of a non-existing identity, or authentic of an existing subject) and synthesizes a new image with the iris texture deformed to match the given new shape. The proposed model preserves the identity and correctly models non-linear deformations of iris muscle. The model synthesizing irises of non-existing subjects is also offered with this paper, which creates a complete pipeline for identity-preserving iris image synthesis and deformation. Images considered in this work conform to selected ISO/IEC 29794-6 quality metrics to make them applicable in biometric systems.

## Abstract

Synthesis of same-identity biometric iris images, both for existing and non-existing identities while preserving the identity across a wide range of pupil sizes, is complex due to intricate iris muscle constriction mechanism, requiring a precise model of iris non-linear texture deformations to be embedded into the synthesis pipeline. This paper presents the first method of fully data-driven, identity-preserving, pupil size-varying synthesis of iris images. This approach is capable of synthesizing images of irises with different pupil sizes representing non-existing identities as well as non-linearly deforming the texture of iris images of existing subjects given the segmentation mask of the target iris image. Iris recognition experiments suggest that the proposed deformation model not only preserves the identity when changing the pupil size but offers better similarity between same-identity iris samples with significant differences in pupil size, compared to state-of-the-art linear and non-linear (bio-mechanical-based) iris deformation models. Two immediate applications of the proposed approach are: (a) synthesis of, or enhancement of the existing biometric datasets for iris recognition, mimicking those acquired

with iris sensors, and (b) helping forensic human experts in examining iris image pairs with significant differences in pupil dilation. Source codes and weights of the models are made available with the paper.

## 1. Introduction

Synthesis of same-identity biometric samples requires algorithms that preserve identity-related features, in addition to the preservation of visual realism of generated images. While realistic-looking irises can be synthesized by either older (non deep learning-based) iris synthesis algorithms [16], or more recently by modern generative models such as Generative Adversarial Networks [31, 32], identity preservation, which involves modeling of complex and nonlinear deformations of the iris pattern when the pupil size changes, is not offered by existing approaches. In this paper we introduce an identity-preserving mechanism that synthesizes same-eye biometric (*i.e.*, compliant with ISO/IEC 19794-6) iris images with varying pupil size, for both non-existing identities and existing iris samples. The proposed model preserves the identity across generated samples, and also offers better biometric performance in the scenario when the

difference in pupil dilation between the probe and gallery samples is significant, compared to a state-of-the-art linear deformation approach [3].

The core novel element of the proposed solution is an autoencoder-based model trained to mimic intricate deformations of iris muscle fibers when the pupil changes its size. This model is fed with an iris image to be deformed and a target iris shape defined by a binary mask indicating new locations of iris pixels. The model deforms the iris pattern to match a new iris shape employing its own “understanding” (learned from the data) of the iris texture deformation phenomenon. We further demonstrate in experiments that this iris texture deformation model offers a better compensation for pupil size variations compared to the linear model [3], dominant in current iris recognition deployments.

The primary advantage of employing deep learning-based models is the elimination of the need for prior assumptions about iris muscle biomechanics, allowing the model to learn these features directly from videos of irises with varying pupil size. The novel contributions of this work are:

- (a) a non-linear iris texture deformation model, operating on biometric (compliant with ISO/IEC 19794-6) iris images, not only preserving the identity but also offering better iris recognition performance when applied to normalize the pupil size compared to the state-of-the-art linear deformation model,
- (b) by adding Generative Adversarial Networks trained to generate ISO-compliant iris images, together with (a) the paper offers a complete method of synthesizing identity-preserving, pupil-size-varying iris images.

Model weights and source codes required to replicate this work are offered with this paper<sup>1</sup>.

## 2. Related Work

### 2.1. Iris Texture Deformation

Several methods have been suggested for both linear and non-linear iris texture deformation, which align iris texture patterns accounting for elastic deformations of the iris muscles. In Daugman’s “rubber sheet” model [3], the annular iris region is stretched to a fixed-sized rectangular block to account for pupil size changes. The limitation of this model lies in its ability to capture only linear deformations, while significant pupil dilation can result in severe deviations from linear movements of the iris pattern. The Wyatt model [30] is a non-linear model based on Rohen’s meshwork [21]<sup>2</sup> designed to minimize iris stretching as the pupil

<sup>1</sup><https://gitfront.io/r/IrisDeform/sk4FaSEQQ5dg/EyePreserve/> (this anonymous repository will be replaced by an actual GitHub repository in the event of paper acceptance)

<sup>2</sup>The iris collagen structure is organized in a series of parallel fibers (arcs) connecting the pupil margin to the iris root (boundary) in clockwise and counterclockwise directions of 90 degrees.

size changes which is achieved by determining the optimal properties of the slopes between two arcs (fibers) and allowing points on a fiber to move only in the radial direction. The model introduced by Yuan and Shi [35] builds upon Wyatt’s iris fiber structure by combining both linear and non-linear techniques and successfully corrects scaling problems resulting from variations in distance. Reyes *et al.* [26] introduced a biomechanical non-linear normalization technique where the iris is conceptualized as a thin cylindrical shell of orthotropic material, and the model calculates iris deformation in the radial direction using stress and strain vectors.

All of the above models were created to be parts of the automatic iris recognition pipeline, rather than to serve as identity-preserving full iris synthesis mechanisms. More recently, Khan *et al.* [10] proposed an autoencoder-based iris texture deformation model, developed and tested on iris images from a single source. Although this model was the first end-to-end, fully deep learning-based model of iris texture deformation, its identity preservation in a cross-dataset setting was not examined.

### 2.2. Synthetic Iris Image Generation

Biometric researchers have recently delved into innovative approaches for iris synthesis, employing deep learning techniques. Yadav *et al.* [32] applied relativistic standard GAN (RaSGAN) to synthesize iris images used later to train iris presentation attack detection methods. This approach, however, did not offer control over the properties of synthesized irises (including the identity-related features). In [31], iWarpGAN was introduced to synthesize iris images not seen during training. It utilizes two distinct input images with different identities and styles. The generated image has a unique identity from the first input image and adopts the style of the second input image. However, its notable limitation is that the number of new synthetic identities is the same as the number of real identities in the dataset.

In general, current generative models can change iris image styles, but none of them, to our knowledge, focuses on preserving the identity (synthetic or real) across different styles.

### 2.3. Identity Preservation in Biometric Data Synthesis

While preserving various object features, usually translating to visual/subjective realism, has been one of the main properties of the image synthesis, the preservation of simultaneously biometric and human perception-assessed features has not yet been widely explored. Tzelepis *et al.* [27] introduced WarpedGANSpace, a method of face synthesis that aims to modify face styles by exploring radial basis function (RBF) paths in a GAN’s latent space. The absence of matching scores for the different face styles does not allow

us to fully assess the fidelity of identity preservation offered by this model.

[14, 15, 24] present controllable GAN models that are capable of generating face images of varying styles while preserving identity. Their models were developed in order to augment face recognition datasets to improve recognition accuracy and generalizability. FaceID-GAN [22], accomplishes the same task by adding a third model (a classifier component) into the GAN training process to encourage same-subject image synthesis. FaceFeat-GAN [23] preserves identity by introducing an intermediate feature generation and curation step before rendering the final image. Other works [34, 37] do not focus on synthesizing biometric data *per se*, but rather on re-stylizing authentic in-the-wild faces to fully frontal, neutral expression images. IP-GAN [33] tries to preserve facial identity while creating caricature faces. Later, [14] leverages a similar concept to keep the identity and pose of the input image while translating it to an image with different appearances and styles. While identity preservation has been studied in face generation, iris image generation is, in a sense, more challenging as the identity information is embedded into higher frequency features.

### 3. Datasets

To enhance the model’s ability to learn non-linear deformations, we selected specific iris datasets with variations in pupil dilation. The existing ISO/IEC 19794-6-compliant iris datasets usually lack samples acquired under intentional ambient light changes to control pupil dilation. We thus acquired samples from four distinct sources (institutions), as outlined in the following subsections.

#### 3.1. Training data

##### 3.1.1 Warsaw BioBase Pupil Dynamics (WBPD)

The WBPD set [11] is composed of 159 high-resolution ( $768 \times 576$  px) iris videos from 42 individuals’ eyes under varying lighting conditions (117,117 iris images in total). During the study, each subject’s eyes were captured at 25 FPS for 30 seconds: the first 15 seconds in darkness, the next 5 seconds in elevated light intensity (pupil constriction period), and the remaining 10 seconds in decreased light intensity (pupil dilation period).

##### 3.1.2 CSOSIPAD

CSOSIPAD is a subset of the “Combined Dataset” iris images introduced by Boyd *et al.* in [1] that was used in conjunction with the WBPD dataset to inject more diversity into the training set for the models. Whereas WBPD had 84 different irises (42 subjects  $\times$  2 eyes), CSOSIPAD added

1,627 distinct irises (each iris can be considered as a different identity).

#### 3.1.3 Training data curation

**WBPD-specific:** Iris images in which the subject was blinking (*i.e.* the iris texture was not visible) were excluded from training. Furthermore, in order to avoid the problem of identity leakage (as described in *e.g.* [25]) and redundancy of very similar images seen during training, images at the beginning of each video (seconds 0-14) were also excluded. After these two exclusions, 55,947 images remained. These images were centrally-cropped to a resolution of  $256 \times 256$ , with 16 pixels of padding on each edge.

**CSOSIPAD-specific:** Samples collected by the LG2200 sensor, which showed interlace artifacts, were removed. The remaining 50,167 CSOSIPAD images were centrally-cropped around the iris in the same manner as the WBPD data and used for subsequent training.

**Common for WBPD and CSOSIPAD:** Our model training requires iris segmentation masks. We utilized the segmentation models from Vance *et al.* [28] to estimate these masks. A further data curation step was necessary to pair small and large pupil images so that we have appropriate inputs and targets to train the deformation model. To achieve this, we first detect and find the pupil and iris radii for all the images in WBPD and CSOSIPAD (again using models from [28]). Previous research showed that the pupil-to-iris ratio usually varies between 0.2 (highly-constricted pupil) and 0.7 (highly-dilated pupil) [4, 26]. Thus, we take all the images with pupil-to-iris ratio between 0.2 and 0.7, and divide them into 5 bins of width 0.1, *i.e.*, the first bin only has images with pupil-to-iris ratios between 0.2 and 0.3, the second bin only has images with pupil-to-iris ratio between 0.3 and 0.4, and so on. For images in each bin, we pair them with images from all the other bins.

Also, we divide the training data into eye-disjoint training and validation sets. This eye-disjoint split is imperative to ensure that the model is learning generic iris muscle movements rather than dynamics specific to subjects present in the training dataset.

#### 3.2. Test data

In addition to the eye-disjoint test set from the WBPD dataset, we use the following three datasets for evaluations.

**Hollingsworth Split (HWS):** The HWS dataset [4] demonstrated that pupil dilation can deteriorate iris biometric performance. The authors utilized this dataset for evaluation and thus, the dataset contains significant pupil dilations for the same identities. So, we employ the same dataset, which is an eye-disjoint subset of CSOSIPAD, in our evaluations.

**Quality-Face/Iris Research Ensemble (Q-FIRE):** The Q-FIRE dataset [6] contains near-infrared (NIR) videos of individuals at different distances and illumination levels. We extract iris images from these videos using simple template-matching techniques and use the resulting dataset for evaluation. The code for extracting this dataset from the Q-FIRE videos are provided along with this paper.

**CASIA-Iris-Lamp (CIL):** The CIL dataset [18], which is available as part of the CASIA-IrisV4 collection, consists of iris images taken using a handheld OKI iris sensor at different illumination levels.

## 4. Iris Texture Deformation Model

### 4.1. Model Overview

To carry out identity-preserving iris texture deformation and get realistic variations of an eye image with different pupil sizes, we train an autoencoder that takes as input a combination of not-deformed iris image and the target iris shape defined by a binary mask to produce the deformed iris image. Fig. 2 provides an overall picture of how this autoencoder is trained.

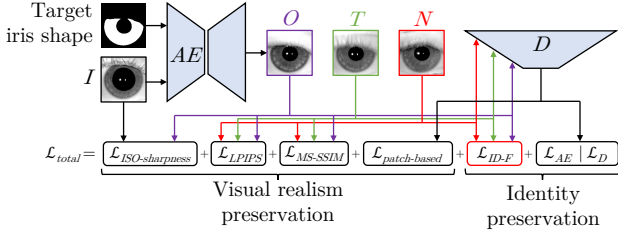


Figure 2. Illustration of the training mechanism with all loss function components explained in Sections 4.1.1 – 4.1.3. Symbols:  $I$  – input image,  $O$  – output image,  $T$  – target sample,  $N$  – negative (impostor) sample,  $D$  – discriminator,  $AE$  – autoencoder.

#### 4.1.1 Identity Preservation

**Filter-based Identity Preservation:** We utilize a filter-based identity preservation loss similar to [10]. Briefly, the Filter-based Identity Loss ( $\mathcal{L}_{ID-F}$ ) between two iris images  $I_1$  and  $I_2$  is defined as:

$$\mathcal{L}_{ID-F}(I_1, I_2) = \|\mathcal{F}_{iris} \otimes N_D(I_1) - \mathcal{F}_{iris} \otimes N_D(I_2)\| \quad (1)$$

where  $N_D$  denotes Daugman’s iris normalization [3],  $\mathcal{F}_{iris}$  denotes a set of iris feature extraction filters,  $\otimes$  denotes the convolution operation and  $\|\cdot\|$  denotes the  $L_1$  norm. To make the filters more comprehensive, we include iris recognition filters from another widely used open-source iris recognition algorithm OSIRIS [19] together with the iris domain-specific human-sourced filters [2] used by [10].

**Adversarial Identity Preservation:** In generative modeling problems with classes of objects, the most commonly used augmentation to the discriminator is to use an auxiliary classifier [17]. Thus, a naive approach would be to treat each identity as a separate class and train an auxiliary classification task with the discriminator. However, this assumes the total number of identities available in the training dataset is the complete set of identities possible which is a wrong assumption to make. To address this, we utilize an adversarial identity loss where the discriminator learns embeddings from random triplets with the same pupil-to-iris ratio and treats the output of the autoencoder as a separate identity pushing its embedding away from the target (anchor) and impostor (negative) identities. On the other hand, the autoencoder learns to produce an image that has the same embedding (from the discriminator) as the target (anchor) image but is different from the impostor (negative) image. We can define this formally as follows. First, let  $\mathcal{L}_{cos}$  be the Cosine Loss which is essentially the opposite of cosine similarity ( $CosSim$ ) scaled to be between 0 and 1 ( $(\mathcal{L}_{cos}(V_1, V_2) = 0.5 \times (1 - CosSim(V_1, V_2)))$ ). Let  $I$  be the input (un-deformed) image,  $T$  be the target image,  $O$  be the output (deformed) image,  $P$  be the positive image that has the same identity as  $I$  and pupil-to-iris ratio as  $T$ ,  $N$  be the negative image that has a different identity but the same pupil-to-iris ratio as  $T$ . Let  $AE$  denote the autoencoder and  $D$  denote the discriminator such that  $D(\cdot)$  represents the embedding for an image. For the loss of the autoencoder  $\mathcal{L}_{AE}$ , we have:

$$\begin{aligned} \mathcal{L}_{AE} = & \mathcal{L}_{cos}(D(O), D(T)) + \mathcal{L}_{cos}(D(O), D(P)) \\ & + \max(\mathcal{L}_{cos}(D(O), D(I)) - margin_{IT}, 0) \quad (2) \\ & + \max(margin_{NT} - \mathcal{L}_{cos}(D(O), D(N)), 0) \end{aligned}$$

where  $margin_{IT} = \mathcal{L}_{cos}(D(I), D(T))$  and  $margin_{NT} = \mathcal{L}_{cos}(D(N), D(T))$ . Thus, to train the autoencoder, firstly we minimize the distance of the output image to both the target and the positive image. Secondly, we also minimize the distance between the output image and the input image as they belong to the same identity but only as much as the loss between input and target, since the input image has a different pupil size than the target. Finally, we maximize the loss between the output and negative images but only as much as the loss between the target and negative images.

For the loss of the discriminator  $\mathcal{L}_D$ , we have:

$$\begin{aligned} \mathcal{L}_D = & \max(\mathcal{L}_{cos}(D(T), D(P)) - \mathcal{L}_{cos}(D(T), D(N)) \\ & + margin_D, 0) \\ & + \max(margin_{NTP} - \mathcal{L}_{cos}(D(O), D(T)), 0) \\ & + \max(margin_{NTP} - \mathcal{L}_{cos}(D(O), D(P)), 0) \\ & + \max(margin_{NTP} - \mathcal{L}_{cos}(D(O), D(N)), 0), \quad (3) \end{aligned}$$

where  $margin_D$  is a hyperparameter that defines the minimum separation required between the anchor and the pos-



itive image, while also specifying the maximum separation that has to be retained between the anchor and the negative image, and  $margin_{NTP}$  is an estimate of the maximum possible loss between impostor pairs of images with same pupil size defined by:

$$margin_{NTP} = \max(margin_{NT}, margin_{NP}) \quad (4)$$

$$margin_{NP} = \mathcal{L}_{cos}(D(N), D(P)). \quad (5)$$

Therefore, at the first part of the loss, we have the classical triplet margin loss formulation between the target, positive, and negative images. This allows the discriminator to learn to distinguish between iris images of different identities. In addition to that, with the subsequent components of the loss, the discriminator learns to distinguish the generated image from the autoencoder as different from the target, positive and negative images.

In summary, the autoencoder and the discriminator are in a minimax game where the autoencoder tries to minimize the distance between embeddings of its output image and the original (target) image while the discriminator tries to maximize this distance while simultaneously learning to distinguish between different identities.

#### 4.1.2 Realism Preservation

**Perceptual Losses (LPIPS and MS-SSIM):** To induce visual realism in the output images, we utilize two different perceptual losses: the Learned Perceptual Image Patch Similarity (LPIPS) loss [36] and Multi-Scale Structural Similarity (MS-SSIM) based loss [29].

**Adversarial Patch Loss:** In our discriminator, we utilize the PatchGAN architecture [5] that only penalizes structure at the scale of patches. That is, this discriminator learns to distinguish each  $N \times N$  patch in an image as real or fake.

**ISO Sharpness Loss:** ISO/IEC 29794-6 SHARPNESS metric utilizes a single filtering kernel engineered to capture frequencies in an iris image that are essential for iris recognition. The ISO-sharpness loss  $\mathcal{L}_{sharp}$  is formulated as follows. Let  $ISO$  be the ISO SHARPNESS score,  $O$  be the output image, and  $In$  be the input image. Then:

$$\mathcal{L}_{sharp}(O, In) = \max(ISO(In) - ISO(O), 0) \quad (6)$$

This loss ensures that the output image has the same or higher ISO SHARPNESS score as the input image provided to the autoencoder.

#### 4.1.3 Triplet Formulation

A direct comparison between output and target images should encourage a model to focus more on features that are common across the images. Thus, especially for losses like

L1 and L2, this method of direct comparison fails to capture distinctive features or encourage high-frequency crispness. Consequently, for all of our comparison-based losses: L1, Filter-based Identity Loss, LPIPS, and MS-SSIM, we employ a triplet-based formulation as defined below.

Let  $\mathcal{L}$  be the loss function,  $O$  be the output image,  $T$  be the target image, and  $Im$  be the impostor image. Then, our triplet-based formulation is as follows:

$$loss = \mathcal{L}(O, T) + \max(margin - \mathcal{L}(O, Im), 0) \quad (7)$$

where

$$margin = \mathcal{L}(T, Im). \quad (8)$$

Our triplet formulation is different from the usual triplet loss formulation in that the margin in the usual triplet loss defines the minimum possible value by which anchor-negative loss should be higher than anchor-positive loss, whereas the margin in our formulation directly defines a value for the minimum possible anchor-negative loss. That is, in our triplet formulation, we utilize the fact that our output image should be as different from the impostor image as the target image should be, and take the loss between the target and the impostor image as the margin.

In summary, through our triplet formulation, by moving the output image away from an impostor image based on how much the target image is different from the impostor while simultaneously moving the output image closer to the target, we encourage the model to generate images with more distinctive features rather than generating a blurry image capturing the common features across images.

#### 4.1.4 Autoencoder Architecture

For our autoencoder architecture, we utilize an Attention-based Nested U-Net architecture similar to [12, 13]. However, we change the upsampling operation from maxpooling to bilinear downsampling to improve the image generation capabilities of the autoencoder. Note that any autoencoder architecture that has adequate image generation capabilities can be plugged in place of the autoencoder architecture we use and it should provide similar results.

## 5. Associated Components

### 5.1. Synthesis of Irises of Non-existing Identities

In order generate synthetic images of non-existent identities, we trained unconditional and conditional (with/without class label) StyleGAN-based models [8, 9].

For the **unconditional** case, a StyleGAN3-based network [9] was trained on the combination of the WBPD and the CSOSIPAD data. Once the training process was complete, a new synthetic iris image could be generated using only a random seed and a corresponding truncation value.

As explained by the original StyleGAN authors, the “truncation trick” allows for balancing image quality with sample diversity. In order to generate a diverse set of realistic-looking synthetic images, a truncation value of 0.5 was used. The resultant images could then be used as the starting input image for the ensuing EyePreserve pipeline.

For the **conditional** case, a StyleGAN2-ADA model [7] was trained on the WBPB data described above. This framework leverages augmentation techniques to expand the training dataset, enabling the training of a model even with a limited amount of data. Images were selected with a pupil-to-iris ratio ranging from 0.2 to 0.7, encompassing the smallest and largest ratios within the WBPB. Next, samples were divided into 7 bins, ensuring that each bin contained a roughly equivalent number of samples, ranging from 7,400 to 7,900. After completing the training of the model, a random latent space vector ( $z$ ) was used in conjunction with a class label (or condition) to generate iris images with different pupil sizes corresponding to the supplied condition. While conditional GANs provide control over selected properties of the image, We found that the identity is not well-preserved as we change the class condition while keeping the latent space vector ( $z$ ) fixed which is illustrated in our evaluation section.

## 5.2. Target Mask Estimation

When we are comparing two iris images, we can deform one of the images to match the pupil size of the other image using the segmentation mask of the latter one using our model. If we simply want to constrict/dilate an iris image given a new pupil “size”, we can detect approximate circles for pupil and iris using models from [28], and generate a circular mask with the new pupil radius. However, this approach would lead to “hallucinated” iris textures if the input iris image is occluded by eyelids. For pupil dilations, a better approach is to cut off a larger pupil circle from the original (input) mask. For pupil constrictions, to avoid hallucinated regions, we may use a more fine-grained segmentation of the iris image (into pupil, iris, and the periocular regions) which enables us to replace the pupil circle with a smaller one while preserving the eyelid boundary.

## 6. Assessment of Identity Preservation

To evaluate the identity-preserving capabilities of our system for both real and synthetic data, we carry out evaluations on different datasets as well as different iris recognition methods. Details about the test datasets are provided in section 3.2.

Our model uses filters from Human-inspired Domain-specific Binarized Image Features (HDBIF) [2] and OSIRIS [19] in training. To ensure that we also evaluate using iris recognition methods fully unseen during train-

ing, we utilize Dynamic Graph Representation for Occlusion Handling in Biometrics (DGR) [20].

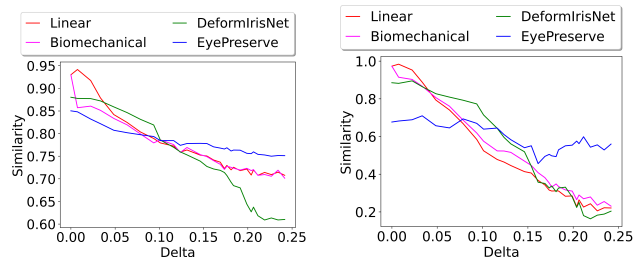
To showcase a measure of standard deviation in our evaluation results and enhance the representation of the comparative analysis among different methods, we randomly sample 10% of our genuine and imposter pairs 100 times with replacement when calculating each Receiver Operating Characteristic (ROC) curves.

## 6.1. Deforming Authentic Irises

### 6.1.1 Scenario: Large Pupil Size Variations

First, we analyze how our model performs with increasing levels of deformation. We utilize the WBPB dataset which was specifically collected to study iris texture deformation due to pupil dynamics and so, contains a wide range of pupil sizes. A simple measure for the degree of pupil size change would be to calculate the difference in the pupil-to-iris ratio ( $\Delta$ ) as was done by Hollingsworth *et al.* [4] ( $\Delta = \|p_1/i_1 - p_2/i_2\|$ , where  $p$  and  $i$  are pupil and iris radii, respectively).  $\Delta$  is very large if one eye has a highly constricted pupil and the other eye has a highly dilated pupil. This value is small if both eyes have a similar pupil size.

For each identity in the test set from WBPB, we compare the iris image with the largest pupil-to-iris ratio (highest dilation) with all the other images. We plot these comparison scores against the  $\Delta$ -values for each iris deformation method. Figure 3 shows the results of these comparisons for one identity in the test set. The curves for the rest of the identities are provided in the supplementary materials. From the graph, we can observe that our model is initially



(a) Comparison of different methods using HDBIF.

(b) Comparison of different methods using DGR.

Figure 3. Comparison of different methods with increasing levels of constriction. HDBIF gives distance scores to pairs of irises and so, the similarity score shown for HDBIF shown here is 1 - score.

worse than linear deformation but it follows a more ‘horizontal’ trajectory. As such, with a large enough change in pupil size, our model starts to perform better than the linear model. We believe this occurs because initially, the error in linear deformation by Daugman’s model and the “actual” non-linear deformation is minute and so, the information loss due to passing the image through the EyePre-

serve model dominates over the accuracy gain from the non-linear deformation done by the EyePreserve. But, as we increase the amount of deformation, the “actual” iris texture deformation becomes significantly different from that estimated by linear deformation and so, the performance of our model overtakes the linear model’s performance. These observations necessitated a need to evaluate our model while considering the degree of change in pupil size for the other datasets as well.

Due to the high fidelity of WBPB data, the low number of identities in the test set, and the filtering that was done to remove almost-closed eyes, HDBIF has an almost 100% Area Under the ROC Curve (AUC) on the test set with any method of iris deformation and, as such, the AUC values for HDBIF does not show much on how the model performs compared to the linear deformation. DGR, however, showcases the changes in AUC as we compare at different ranges of  $\Delta$ . Table 1 summarizes the results from DGR using WBPB. The results we observe here also illustrate that our model works better at larger iris texture deformations.

Table 1. Comparison of AUCs averaged over 100 samples with replacements consisting of 10% of the DGR comparison scores on the WBPB test set for different bins of  $\Delta$ . The standard deviation  $\epsilon \in [0.001, 0.002]$  in all variants.

$\Delta$	Linear	Biomech	EyePreserve	
			Dilate	Constrict
[0, 0.1]	0.996 $\pm$ $\epsilon$	0.995 $\pm$ $\epsilon$	0.996 $\pm$ $\epsilon$	0.995 $\pm$ $\epsilon$
(0.1, 0.2]	0.994 $\pm$ $\epsilon$	0.995 $\pm$ $\epsilon$	0.984 $\pm$ $\epsilon$	0.992 $\pm$ $\epsilon$
(0.2, 0.3]	0.991 $\pm$ $\epsilon$	0.991 $\pm$ $\epsilon$	0.992 $\pm$ $\epsilon$	0.995 $\pm$ $\epsilon$
(0.3, 0.4]	0.986 $\pm$ $\epsilon$	0.985 $\pm$ $\epsilon$	0.996 $\pm$ $\epsilon$	0.995 $\pm$ $\epsilon$

It has been shown that the biomechanical model of iris texture deformation [26] performs about the same as the linear deformation [10]. Also, in our analyses above, we observed that the biomechanical model has very similar scores compared to the scores from linear deformation (the score lines in the  $\Delta$ -based curves are usually closely intertwined and the AUC values are really close). Thus, in the rest of our evaluations, we opt to compare our method with the more widely employed Daugman’s linear deformation method instead of the biomechanical model.

### 6.1.2 Scenario: Moderate Pupil Size Variations

To further analyze how our model performs with pupil size variations, we utilize the HWS dataset. The pupil variation was achieved in this dataset by turning the ambient lighting off during the collection which means that the iris muscles were not taken through their full range of motion. As such, the range of  $\Delta$ -values is not as high as we find in the WBPB dataset. In [4], to evaluate the effects of different levels of dilation, Hollingsworth *et al.* separated the comparison pairs into sets of  $\Delta$  values ranging from 0 to 0.4 where each set had a width of 0.1. However, they state the number of comparison pairs in the set 0.3-0.4 was extremely low.

First, we consider the case where the change in pupil size is high. In particular, we only take pairs where  $\Delta \geq 0.2$ . This is motivated by the fact that HWS has very few pairs with  $\Delta > 0.3$ . We find that our approach performs better than the classical Daugman’s normalization when we are constricting the pupil. We believe this is happening because when we are dilating the pupil using our model, we are essentially compressing the iris information into a smaller space and then, we are polar-normalizing using Daugman’s model into a rectangular region to be used in our matchers. This could lead to a loss of features that are used by the iris matchers. The linear compensation in the way it is evaluated here does not suffer from this as we only carry out polar-normalization and therefore, directly move to this rectangular region.

Secondly, we also check the performance of our model when there is little or no change in pupil size. We expect the classical approach to work better here as there is no significant iris texture deformation that our model can ‘fix’ and, moreover, passing the image through the network can introduce noise/blurriness into the images. We observe that the performance after passing through our deformation model is almost the same as using the original images showcasing that the amount of noise/blurriness introduced is quite low. Table 2 showcases the performance of our model for both scenarios described above.

In our analysis, DeformIrisNet [10] does not generalize well to new datasets. While it performs well on the WBPB dataset, its performance on HWS is significantly worse. Overall, complementary to what we saw in our analysis with increasing levels of deformation in the previous section, we observe that our model performs better in terms of iris recognition when the iris texture deformation is large. Also, as in the previous section, we observe that pupil constriction with our model usually performs better in terms of iris recognition than pupil dilation as the compression of information due to pupil dilation most likely deteriorates iris matcher performance.

### 6.1.3 Scenario: Small Pupil Size Variations

We also consider two other datasets for our evaluations: Q-FIRE and CIL. While these datasets contain pupil size variation, they do not have comparisons with large  $\Delta$ . The split of data with  $\Delta \geq 0.2$  is not statistically significant for either of these datasets. As such, we provide an overall evaluation results on these datasets. Table 2 presents our findings in these datasets. The good performance of our model in the HDBIF method but not on the DGR could most likely be due to “hallucinated” textures when the target mask is larger (has more eyelid opening) than the input image. We use the original polar-normalized mask in HDBIF which discards any “dreamed-up” textures during comparison.

Table 2. Comparison of AUCs averaged over 100 samples with replacements consisting of 10% of the comparison score for HDBIF and DGR on HWS (separated by  $\Delta$ ), Q-FIRE, and CIL.

	HWS ( $\Delta \geq 0.2$ )		HWS ( $\Delta \leq 0.1$ )		Q-FIRE		CIL	
	HDBIF	DGR	HDBIF	DGR	HDBIF	DGR	HDBIF	DGR
Linear	0.9954 $\pm$ 0.0021	0.9726 $\pm$ 0.0084	0.9965 $\pm$ 0.0011	0.9910 $\pm$ 0.0020	0.9947 $\pm$ 0.0006	0.9762 $\pm$ 0.0043	0.9984 $\pm$ 0.0002	0.9864 $\pm$ 0.0007
Ours	Dilate	0.9860 $\pm$ 0.0051	0.9658 $\pm$ 0.0127	0.9935 $\pm$ 0.0016	0.9898 $\pm$ 0.0019	0.9957 $\pm$ 0.0004	0.9551 $\pm$ 0.0035	0.9972 $\pm$ 0.0002
	Constrict	0.9962 $\pm$ 0.0023	0.9827 $\pm$ 0.0071	0.9944 $\pm$ 0.0014	0.9898 $\pm$ 0.0022	0.9962 $\pm$ 0.0014	0.9577 $\pm$ 0.0042	0.9984 $\pm$ 0.0001
DeformIrisNet	0.6830 $\pm$ 0.0201	0.6996 $\pm$ 0.0297	0.6290 $\pm$ 0.0118	0.6908 $\pm$ 0.0146				

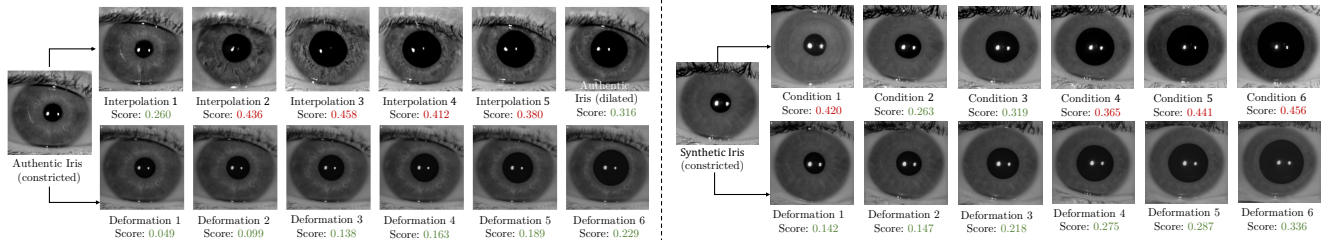


Figure 4. Generating synthetic iris images with different pupil-to-iris size ratios ( $\Delta$ ) for two scenarios: 1) interpolating the new pupil size between two given iris images (**left section**), and 2) changing the pupil size for a single iris image (**right section**). Upper rows demonstrate failures in identity preservation by a standard GAN, which was used to generate samples based on a linear interpolation in the GAN’s latent space between two iris image projections (upper left row), and by a conditional GAN, which was used to generate samples with the pupil size as a “condition” (upper right row). HDBIF scores shown in green (match) or red (non-match) are calculated between the left images and the synthesized samples.

## 6.2. Synthetic Irises

**Unconditional StyleGAN:** Although GANs have shown the ability to generate highly realistic-looking iris images [25, 31], the inner workings of these GANs’ latent spaces are neither known nor predictable in the synthetic iris domain. For instance, linearly interpolating between small- and large-pupil images of the same iris in the StyleGAN’s latent space  $W$  (as demonstrated in left section of Fig. 4) does not preserve identity. Although the endpoints of this interpolation process are images of the same iris, the intermediate interpolated images show iris textures that (a) do not match either endpoint, and (b) are recognizably fake. Contrarily, the proposed EyePreserve approach (bottom row), succeeds in maintaining identity for varying pupil dynamics, as can be seen in the green HDBIF scores.

**Conditional StyleGAN:** Conditional GANs also struggle to preserve identity, especially in the case of highly dilated irises. They also generate synthetic iris images similar to identities seen during training. As depicted in the right section of Fig. 4, this model failed to generate iris images with preserved identity using the same latent code  $z$  but different conditions and, moreover, our EyePreserve model consistently produced images with better matching scores for each condition.

## 7. Conclusions

The pupil oscillates its size with a frequency between 0.5 and 2.0 Hz and a low amplitude, even if ambient light inten-

sity does not change (this phenomenon is known as *hippus*), and larger pupil dilation changes are observed for varying light changes. Such changes are one of the most important factors contributing to within-class variance in iris recognition. However, complex iris texture deformations are difficult to model and require strong anatomical assumptions. This paper proposes the first deep learning-based non-linear iris deformation model that generalizes well, along with a complete iris synthesis toolkit, which preserves identity when deforming the iris texture. The proposed model learns the visual appearance of the intricate iris muscle deformations without a need for often oversimplified anatomical assumptions and learns them quite effectively offering better performance of tested iris recognition methods compared to a state-of-the-art linear and non-linear (bio-mechanical-based) iris texture deformation models for significant differences in pupil dilation. This work advances iris recognition field in several ways: (a) offers better compensation of pupil dilation translating to better recognition performance compared to state-of-the-art models, (b) by correct alignment of iris features it serves better the emerging field of forensic human experts-based iris examination, (c) it offers a complete pipeline of identity-preserving ISO/IEC-19794-6-compliant iris image synthesis, potentially enhancing recognition and presentation attack detection datasets.

## References

- [1] Aidan Boyd, Jeremy Speth, Lucas Parzianello, Kevin W. Bowyer, and Adam Czajka. Comprehensive study in open-set iris presentation attack detection. *IEEE Transactions on*



- Information Forensics and Security*, 18:3238–3250, 2023. 3
- [2] Adam Czajka, Daniel Moreira, Kevin Bowyer, and Patrick Flynn. Domain-specific human-inspired binarized statistical image features for iris recognition. In *2019 IEEE Winter Conference on Applications of Computer Vision (WACV)*, pages 959–967. IEEE, 2019. 4, 6
- [3] John G Daugman. High confidence visual recognition of persons by a test of statistical independence. *IEEE Trans. Pattern Anal. Mach. Intell.*, 15(11):1148–1161, 1993. 2, 4
- [4] Karen Hollingsworth, Kevin W Bowyer, and Patrick J Flynn. Pupil dilation degrades iris biometric performance. *Computer Vision and Image Understanding*, 113(1):150–157, 2009. 3, 6, 7
- [5] Phillip Isola, Jun-Yan Zhu, Tinghui Zhou, and Alexei A Efros. Image-to-image translation with conditional adversarial networks. In *IEEE/CVF International Conference on Computer Vision and Pattern Recognition (CVPR)*, pages 1125–1134, 2017. 5
- [6] P. A. Johnson, P. Lopez-Meyer, N. Sazonova, F. Hua, and S. Schuckers. Quality in face and iris research ensemble (q-fire). In *2010 Fourth IEEE International Conference on Biometrics: Theory, Applications and Systems (BTAS)*, pages 1–6, 2010. 4
- [7] Tero Karras, Miika Aittala, Janne Hellsten, Samuli Laine, Jaakko Lehtinen, and Timo Aila. Training generative adversarial networks with limited data. In *Proc. NeurIPS*, 2020. 6
- [8] Tero Karras, Miika Aittala, Janne Hellsten, Samuli Laine, Jaakko Lehtinen, and Timo Aila. Training generative adversarial networks with limited data. *Advances in Neural Information Processing Systems*, 33:12104–12114, 2020. 5
- [9] Tero Karras, Miika Aittala, Samuli Laine, Erik Härkönen, Janne Hellsten, Jaakko Lehtinen, and Timo Aila. Alias-free generative adversarial networks. *Advances in Neural Information Processing Systems*, 34:852–863, 2021. 5
- [10] Siamul Karim Khan, Patrick Tinsley, and Adam Czajka. Deformirisnet: An identity-preserving model of iris texture deformation. In *IEEE Winter Conference on Applications of Computer Vision (WACV)*, pages 900–908, 2023. 2, 4, 7
- [11] Jeffery Kinnison, Mateusz Trokielewicz, Camila Carballo, Adam Czajka, and Walter Scheirer. Learning-free iris segmentation revisited: A first step toward fast volumetric operation over video samples. In *2019 International Conference on Biometrics (ICB)*, pages 1–8. IEEE, 2019. 3
- [12] Chen Li, Yusong Tan, Wei Chen, Xin Luo, Yuanming Gao, Xiaogang Jia, and Zhiying Wang. Attention Unet++: A nested attention-aware u-net for liver CT image segmentation. In *2020 IEEE International Conference on Image Processing (ICIP)*, pages 345–349. IEEE, 2020. 5
- [13] Chen Li, Yusong Tan, Wei Chen, Xin Luo, Yulin He, Yuanming Gao, and Fei Li. Anu-net: Attention-based nested u-net to exploit full resolution features for medical image segmentation. *Computers & Graphics*, 90:11–20, 2020. 5
- [14] Tingting Li, Huan Zhao, Jing Huang, and Keqin Li. Cross-domain image translation with a novel style-guided diversity loss design. *Knowledge-Based Systems*, 255:109731, 2022. 3
- [15] Feng Liu, Minchul Kim, Anil Jain, and Xiaoming Liu. Controllable and guided face synthesis for unconstrained face recognition. In *European Conference on Computer Vision*, pages 701–719. Springer, 2022. 3
- [16] Sarvesh Makthal and Arun Ross. Synthesis of iris images using markov random fields. In *2005 13th European Signal Processing Conference*, pages 1–4, 2005. 1
- [17] Augustus Odena, Christopher Olah, and Jonathon Shlens. Conditional image synthesis with auxiliary classifier gans. In *International Conference on Machine Learning*, pages 2642–2651. PMLR, 2017. 4
- [18] Institute of Automation at the Chinese Academy of Sciences. CASIA-IrisV4. <http://biometrics.idealtest.org/dbDetailForUser.do?id=4#/datasetDetail/4>, 2020. Dataset published by the Chinese Academy of Sciences’ Institute of Automation. 4
- [19] Nadia Othman, Bernadette Dorizzi, and Sonia Garcia-Salicetti. Osiris: An open source iris recognition software. *Pattern Recognition Letters*, 82:124–131, 2016. 4, 6
- [20] Min Ren, Yunlong Wang, Zhenan Sun, and Tieniu Tan. Dynamic graph representation for occlusion handling in biometrics. In *AAAI*, pages 11940–11947, 2020. 6
- [21] H Rohen. Der bau der regenbogenhaut beim menschen und einigen säugern. *Gegenbaur Morphology Journal*, 91:140–181, 1951. 2
- [22] Yujun Shen, Ping Luo, Junjie Yan, Xiaogang Wang, and Xiaou Tang. Faceid-gan: Learning a symmetry three-player gan for identity-preserving face synthesis. In *IEEE/CVF International Conference on Computer Vision and Pattern Recognition (CVPR)*, pages 821–830, 2018. 3
- [23] Yujun Shen, Bolei Zhou, Ping Luo, and Xiaou Tang. Facefeat-GAN: a two-stage approach for identity-preserving face synthesis. *arXiv preprint arXiv:1812.01288*, 2018. 3
- [24] Alon Shoshan, Nadav Bhonker, Igor Kviatkovsky, and Gerard Medioni. GAN-control: Explicitly controllable GANs. In *IEEE International Conference on Computer Vision (ICCV)*, pages 14083–14093, 2021. 3
- [25] Patrick Tinsley, Adam Czajka, and Patrick J Flynn. Haven’t i seen you before? assessing identity leakage in synthetic irises. In *2022 IEEE International Joint Conference on Biometrics (IJCB)*, pages 1–9. IEEE, 2022. 3, 8
- [26] Inmaculada Tomeo-Reyes, Arun Ross, Antwan D Clark, and Vinod Chandran. A biomechanical approach to iris normalization. In *2015 International Conference on Biometrics (ICB)*, pages 9–16. IEEE, 2015. 2, 3, 7
- [27] Christos Tzelepis, Georgios Tzimiropoulos, and Ioannis Patras. Warpedganspace: Finding non-linear rbf paths in gan latent space. In *Proceedings of the IEEE/CVF International Conference on Computer Vision*, pages 6393–6402, 2021. 2
- [28] Nathan Vance, Jeremy Speth, Siamul Khan, Adam Czajka, Kevin W. Bowyer, Diane Wright, and Patrick Flynn. Deception detection and remote physiological monitoring: A dataset and baseline experimental results. *IEEE Transactions on Biometrics, Behavior, and Identity Science*, 4(4):522–532, 2022. 3, 6
- [29] Zhou Wang, Eero P Simoncelli, and Alan C Bovik. Multiscale structural similarity for image quality assessment. In

- The Thirty-Seventh Asilomar Conference on Signals, Systems & Computers, 2003*, pages 1398–1402. Ieee, 2003. 5
- [30] Harry J Wyatt. A ‘minimum-wear-and-tear’ meshwork for the iris. *Vision Research*, 40(16):2167–2176, 2000. 2
- [31] Shivangi Yadav and Arun Ross. iWarpGAN: Disentangling Identity and Style to Generate Synthetic Iris Images. *arXiv preprint arXiv:2305.12596*, 2023. 1, 2, 8
- [32] Shivangi Yadav, Cunjian Chen, and Arun Ross. Synthesizing iris images using rasgan with application in presentation attack detection. In *2019 IEEE/CVF Conference on Computer Vision and Pattern Recognition Workshops (CVPRW)*, pages 2422–2430, 2019. 1, 2
- [33] Lan Yan, Wenbo Zheng, Chao Gou, and Fei-Yue Wang. Ip-gan: Identity-preservation generative adversarial network for unsupervised photo-to-caricature translation. *Knowledge-Based Systems*, 241:108223, 2022. 3
- [34] Xi Yin, Xiang Yu, Kihyuk Sohn, Xiaoming Liu, and Manmohan Chandraker. Towards large-pose face frontalization in the wild. In *IEEE International Conference on Computer Vision (ICCV)*, pages 3990–3999, 2017. 3
- [35] Xiaoyan Yuan and Pengfei Shi. A non-linear normalization model for iris recognition. In *International Workshop on Biometric Person Authentication*, pages 135–141. Springer, 2005. 2
- [36] Richard Zhang, Phillip Isola, Alexei A Efros, Eli Shechtman, and Oliver Wang. The unreasonable effectiveness of deep features as a perceptual metric. In *IEEE/CVF International Conference on Computer Vision and Pattern Recognition (CVPR)*, 2018. 5
- [37] Xiangyu Zhu, Zhen Lei, Junjie Yan, Dong Yi, and Stan Z Li. High-fidelity pose and expression normalization for face recognition in the wild. In *IEEE Trans. Pattern Anal. Mach. Intell.*, pages 787–796, 2015. 3

# EyePreserve: Identity-Preserving Iris Synthesis

## Supplementary Material

### 8. Introduction

This document presents the supplementary materials omitted from the main paper due to space limitations. In Section 9, we provide more visual and score comparisons for synthetic irises from the conditional GAN. In Section 10, we provide histograms for the genuine and imposter distributions of our evaluation scores for authentic irises. Our code is available here: <https://gitfront.io/r/IrisDeform/sk4FaSEQQ5dg/EyePreserve/>

### 9. Additional visualizations for synthetic irises

We provide additional comparisons with the conditional GAN in figures 5 and 6. The conditional GAN can sometimes produce irises of completely different identities as shown in 5. Our method is able to preserve the identity that is provided as input across the different pupil sizes. In the figure 5, we can see that for the above case where condition 0 of the conditional GAN is the input, our method is able to preserve the identity in this generated iris image across the different pupil dilations. Similarly, our method is also able to preserve the identity in the generated iris image from condition 7 (which is the most dilated version of the iris

image from condition 0 and is drastically different visually but ideally it shouldn't have been) across the different pupil constrictions. In figure 6, we show a “cherry-picked” sample from conditional GAN that produces iris images that are “similar” (looks visually similar and have identities that are not drastically different). However, our method is able to “better” preserve identity as indicated by the lower HDBIF distance scores across the different conditions.

### 10. Histograms for authentic iris comparison scores

We provide the histograms of genuine and imposter scores for HDBIF and DGR in the WBPB test set in figures 7 and 8. We also provide the decidability score ( $d'$ ) with each graph. We find that the scores for our method have a higher separation than linear in nearly all cases as indicated by the higher  $d'$  (one thing to note is that  $d'$  assumes the genuine and imposter distributions to be Gaussian). Another interesting thing we see is an overall shift in all (similarity) scores to the right. We believe this happens due to “similar” noise introduced by the neural network which makes all comparisons (genuine or imposter) have a higher similarity score than unprocessed images.

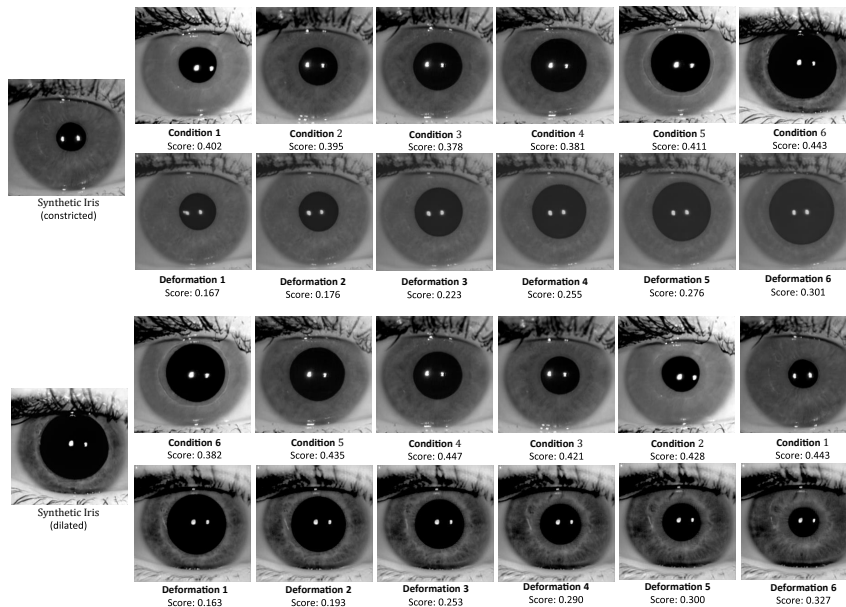


Figure 5. The figure shows a sample for the conditional GAN where all the iris images for the same latent vector  $z$  across the different pupil size conditions look quite different from each other (and therefore, are of different identities with high HDBIF distance scores from each other). We show the cases of both pupil dilation (above) and constriction (below) with our model. The conditional GAN images are the same in each case but are just rearranged to make it easier for comparison. We can see that our deformation model preserves the identity of its input across the different pupil sizes.

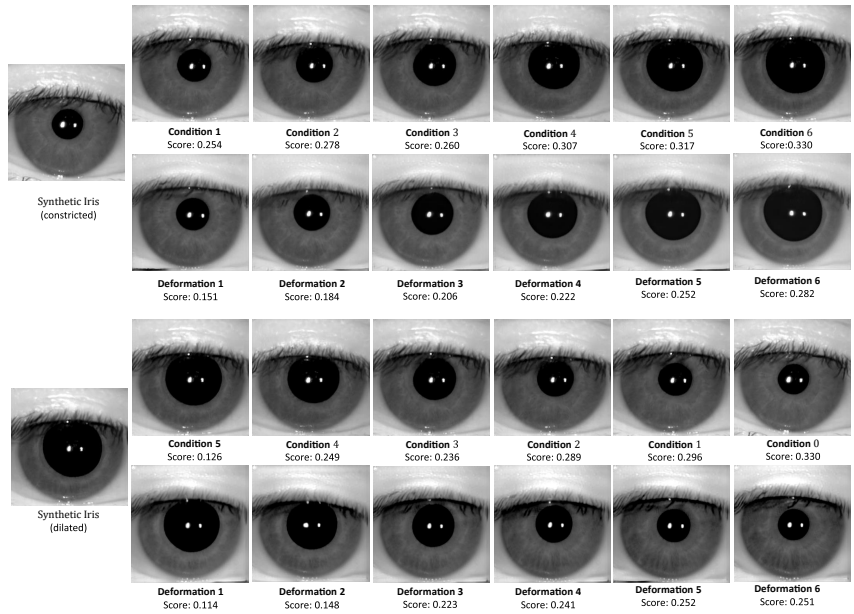


Figure 6. The figure shows a “cherry-picked” sample for the conditional GAN where the iris images generated look quite similar for the same latent vector  $z$  across the different pupil size conditions. We show the cases of both pupil dilation (above) and constriction (below) with our model. The conditional GAN images are the same in each case but are just rearranged to make it easier for comparison. We can see that our deformation model always gives closer HDBIF distance scores and, therefore, is able to better preserve identity while changing pupil sizes.

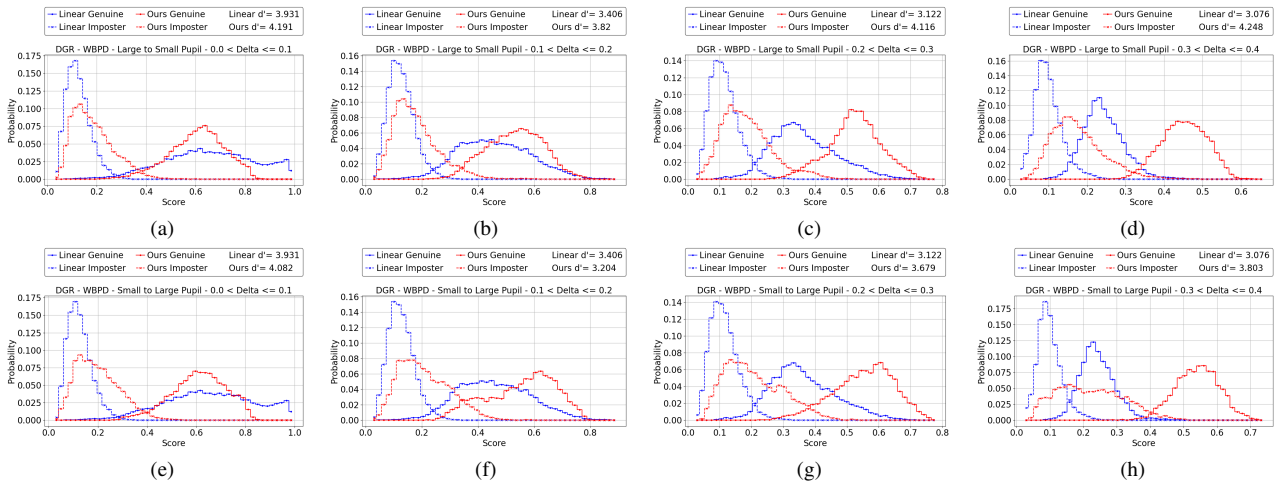


Figure 7. The figures above show the histograms of scores for DGR. (a)-(d) shows the scores for pupil constriction with (a) showing values for  $\Delta$  range: 0 to 0.1, (b) showing values for  $\Delta$  range: 0.1 to 0.2 and so on. (e)-(h) shows the scores for pupil dilation with (e) showing values for  $\Delta$  range: 0 to 0.1, (f) showing values for  $\Delta$  range: 0.1 to 0.2 and so on.



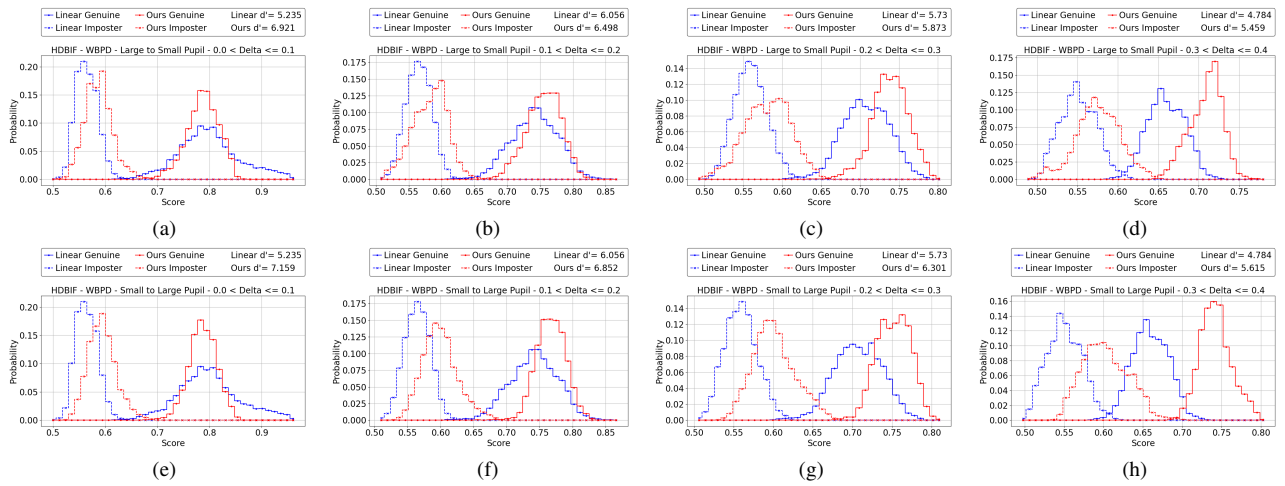


Figure 8. The figures above show the histograms of scores for HDBIF (The scores are shown as “similarity” thus, is 1 - HDBIF score). (a)-(d) shows the scores for pupil constriction with (a) showing values for  $\Delta$  range: 0 to 0.1, (b) showing values for  $\Delta$  range: 0.1 to 0.2 and so on. (e)-(h) shows the scores for pupil dilation with (e) showing values for  $\Delta$  range: 0 to 0.1, (f) showing values for  $\Delta$  range: 0.1 to 0.2 and so on.